Molecular origins of induction and loss of photoinhibition-related energy dissipation q I

Wojciech J Nawrocki, Xin Liu, Bailey Raber, Chen Hu, Catherine de Vitry, Doran Bennett, Roberta Croce

PLANT SCIENCES

Molecular origins of induction and loss of photoinhibition-related energy dissipation q_I

Wojciech J. Nawrocki[1,2]*, Xin Liu[1,2], Bailey Raber[3], Chen Hu[1,2], Catherine de Vitry[4], Doran I. G. Bennett[3], Roberta Croce[1,2]*

Photosynthesis fuels life on Earth using sunlight as energy source. However, light has a simultaneous detrimental effect on the enzyme triggering photosynthesis and producing oxygen, photosystem II (PSII). Photoinhibition, the light-dependent decrease of PSII activity, results in a major limitation to aquatic and land photosynthesis and occurs upon all environmental stress conditions. In this work, we investigated the molecular origins of photoinhibition focusing on the paradoxical energy dissipation process of unknown nature coinciding with PSII damage. Integrating spectroscopic, biochemical, and computational approaches, we demonstrate that the site of this quenching process is the PSII reaction center. We propose that the formation of quenching and the closure of PSII stem from the same event. We lastly reveal the heterogeneity of PSII upon photoinhibition using structure-function modeling of excitation energy transfer. This work unravels the functional details of the damage-induced energy dissipation at the heart of photosynthesis.

INTRODUCTION

Oxygenic photosynthesis supplies virtually the entire biosphere with chemical energy and oxygen. The first steps of this process involve light harvesting and H_2O oxidation by photosystem II (PSII), the water:plastoquinone photooxidoreductase. PSII is arranged in supercomplexes in the appressed regions of the thylakoid membranes within plant and algal chloroplasts (*1*). In the model green alga *Chlamydomonas reinhardtii*, these multimeric, pigment-protein supercomplexes consist of (i) PSII core: composed of the reaction center (RC) complex (the D1 and D2 proteins, cytochrome b_{559} and PsbI), the CP43 and CP47 antennae, the luminal proteins PsbO, P, and Q, stabilizing the oxygen-evolving Mn_4CaO_5 cluster (OEC), and 10 other small transmembrane subunits; (ii) the minor antennae CP26 and CP29; and (iii) the light-harvesting complex II (LHCII) (*2*, *3*). The antennae greatly enhance the absorption cross section of PSII, allowing efficient light harvesting and excitation energy transfer to the RC, where charge separation takes place and electron transfer begins. The antenna complexes also link different RCs, allowing the excitation to travel in the membrane until it is used to drive stable photochemistry (*4*, *5*). However, both the charge-separated states and the long-lived chlorophyll excitation are potentially detrimental to PSII because of oxygen sensitization. PSII has adapted to minimize reactive oxygen species (ROS) formation thanks to the heterodimeric RC complex design, redox tuning (*6*–*8*), and auxiliary mechanisms that dissipate a fraction of the excitation (*9*, *10*). The latter principally describes energy quenching, termed q_E nonphotochemical quenching (NPQ), which in *Chlamydomonas* is mediated by the LHCSR3 antenna after protonation of its lumen-exposed residues (*9*, *11*). In addition, PSII regulates its absorption cross section via the process of state transitions, a phosphorylation-dependent antenna redistribution between PSII and PSI (*12*, *13*). These mechanisms can decrease the probability of PSII damage, known as photoinhibition.

Known for more than six decades, photoinhibition is a process of slowly recovering, light-induced decrease of PSII activity (*14*). It causes inactivation of the RC and damage to the D1 protein (*15*, *16*), which is then degraded and repaired by de novo synthesis (*17*–*20*). Crucially, photoinhibition is a major limiting factor to both terrestrial and aquatic photosyntheses (*21*), and PSII function impairment is particularly strong when high light (HL) is combined with other environmental stresses (*18*). It is thus expected to increase as a result of climate change and negatively affect crop productivity (*22*).

Two mechanisms of photoinhibition likely take place in vivo depending on the incident light spectrum (*23*). As demonstrated in the works of Tyystjärvi and Murata groups (*19*, *24*, *25*), the first of them is a process where the donor side of PSII (the OEC) becomes damaged independently of PSII photochemistry and is induced by blue/ultraviolet (UV) light. Furthermore, an independent, oxidative damage mechanism is correlated with the rate of photosynthetic reactions (*19*, *26*), its action spectrum following chlorophyll absorbance, and it can be partly alleviated by photoprotection mechanisms. In both cases, NPQ allows PSII repair to proceed efficiently thanks to a decrease of ROS formation (*10*, *24*, *25*). Photoinhibition thus illustrates the dilemma between optimization of photosynthesis and excess energy management.

Unexpectedly, photoinhibition itself is associated with a decrease in chlorophyll fluorescence yield (*27*–*30*). This behavior is unexpected because in other conditions where PSII is inactive or absent [e.g., in the absence of electron acceptors (*31*, *32*), in the presence of the herbicide DCMU blocking PSII acceptor side (*33*), in the PSII RC knockout mutant (*34*), and when only LHCs accumulate in the thylakoids (*35*)], the fluorescence level is high [average Chl* lifetime of >1.2 ns; e.g., (*11*)], because of the lack of photochemical quenching from charge-separating PSII. The site of q_I, the quenching species, the mechanism, and the role of the energy dissipation related to photoinhibition are at present unknown.

To study photoinhibition and the related quenching, we used an integrated approach in vivo. Multiscale analysis of fluorescence changes from picoseconds to hours provided information about q_I

[1]Biophysics of Photosynthesis, Department of Physics and Astronomy, Faculty of Science, Vrije Universiteit Amsterdam, 1081 HV Amsterdam, Netherlands. [2]LaserLaB Amsterdam, Vrije Universiteit Amsterdam, 1081 HV Amsterdam, Netherlands. [3]Department of Chemistry, Southern Methodist University, P.O. Box 750314, Dallas, TX, USA. [4]Institut de Biologie Physico-Chimique, UMR 7141, CNRS-Sorbonne Université, 75005 Paris, France.
*Corresponding author. Email: w.j.nawrocki@vu.nl (W.J.N.); r.croce@vu.nl (R.C.)

and the extent of photodamage of the photosynthetic apparatus. The use of a range of mutants allowed us to pinpoint the location of q_I and the mechanism of its formation and loss. Last, we used membrane-scale modeling of energy excitation transfer to reveal the extent of heterogeneity in PSII populations upon photoinhibition.

RESULTS

Loss of fluorescence upon HL treatment

The protocol used throughout the study to investigate the origin of the slowly reversible chlorophyll fluorescence decrease upon HL treatment in *Chlamydomonas* is shown in Fig. 1A. To focus exclusively on the photoinhibition-related effect, the experiments were performed in the absence of q_E (using cells not previously exposed to HL, which thus do not contain LHCSR), PSII repair (D1 resynthesis was blocked with lincomycin), and initially in the *stt7-9* strain, which is unable to perform state transitions (*36*).

Throughout the 90 min of HL treatment (1500 µmol photons m^{-2} s^{-1}), the maximal fluorescence yield of the cells (F_M, where the PSII RCs are in closed state) decreased to below 50% of its initial value (Fig. 1B and fig. S1), while the dark-adapted fluorescence value (F_0, PSII RCs in open state) increased (Fig. 1B). The latter observation suggests that quenching coincides with the closing of PSII RCs upon photodamage or with the detachment of the antenna, because if only quenching occurred, F_0 would also decrease. The F_V/F_M parameter, often used to quantify the extent of PSII damage, strongly correlated with the decrease in oxygen evolution capacity, confirming photoinhibition of PSII during the HL treatment. PSI was instead little affected by the treatment, as demonstrated by the small decrease of the amplitude of photooxidizable P_{700} (fig. S2).

Fluorescence quenching is a term that describes an increase in the overall rate of nonradiative excited state decay. It needs to be distinguished from a decrease of fluorescence caused by a decrease in absorption. The observed reduction in F_M is on a time scale of <2 hours an energy quenching process, as indicated by the decrease in fluorescence lifetime of the cells (Fig. 1C and fig. S3C) and the fact that the absorption capacity of the cells decreased only slightly during the HL treatment (fig. S1). This quenching process is thus hereafter termed q_I.

Site of the q_I quenching

There exist several possible quenching sites in the thylakoid membranes of *Chlamydomonas*. These include (i) PSI [which can act as a quencher of PSII when the two complexes are in close contact (*37*)]; (ii) LHCII [as proposed for q_E in vascular plants (*38*)]; (iii) LHCSR [the site of the pH-dependent quenching (*11*)]; and (iv) the PSII core itself (through an unknown mechanism). To identify the q_I site, we used a combination of genetic and spectroscopic approaches.

First, time-resolved fluorescence measurements were performed before (0-min HL) and after 20 and 90 min of HL treatment to investigate photoinhibition-dependent changes in spectra and lifetimes of the lincomycin-treated cells (Fig. 1C). Three decay components were sufficient to describe the fluorescence kinetics at each time point. The decay-associated spectra are shown in Fig. 1D. Before photoinhibition, the two longer components, with lifetimes $\tau_3 = 1.76$ ns and $\tau_2 = 219$ ps, were associated with PSII, while the shortest component

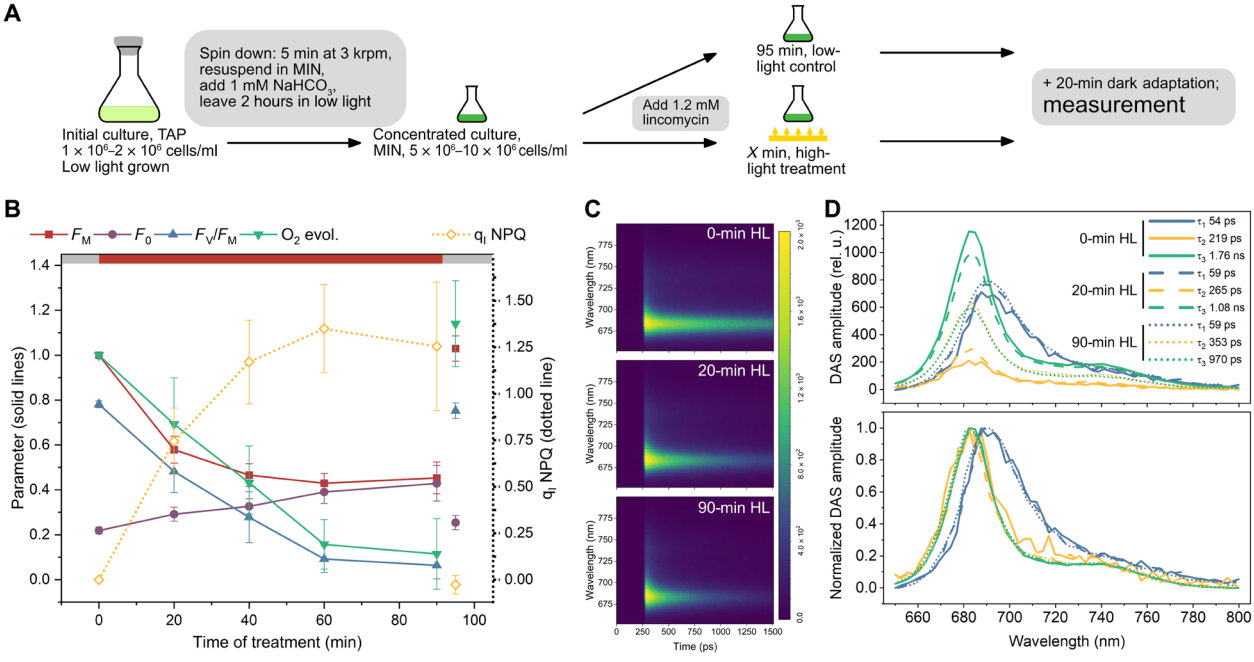

Fig. 1. Decrease of chlorophyll fluorescence following photoinhibition in vivo is a quenching. (**A**) Scheme of the treatment before the measurements. TAP, tris-acetate-phosphate medium; MIN, tris-phosphate medium. (**B**) Quantification of the changes in relevant parameters throughout the HL treatment in the *stt7-9* strain. The last time point (95 min) represents the value in samples treated with lincomycin but not exposed to HL. $n = 6 \pm$ SD. (**C**) Two-dimensional maps of time-resolved fluorescence data of the *stt7-9* strain at $t = 0$, 20, and 90 min of HL treatment, detected with a Streak camera setup. False coloring depicts the intensity (number of photons) in each bin. A representative dataset is shown. (**D**) Decay-associated spectra (DAS) of the data in (C). Top: The sums of spectra integrals at $t = 20$ and 90 min were normalized to the $t = 0$ sum. Lifetimes and spectra were free parameters of linked fitting of three biological replicas of the experiment (in total, nine images; see analysis of the other replicas in fig. S15 and fitting quality in figs. S16 to S18).

had spectrum and lifetime (τ_1 = 54 ps) typical of PSI. After 90-min HL treatment, the amplitude and lifetime of the longer PSII component decreased, and those of the shorter PSII component increased. Crucially, no noticeable differences were observed in their spectra (Fig. 1D). The absence of additional emitting species after HL treatment, in particular one with a red-shifted spectrum, suggests that LHC aggregation is not the mechanism behind q_I (*39*), and absence of blue shift indicates that antenna detachment does not take place upon photoinhibition and observed F_0 rise has another origin. The PSI spectra and lifetimes were similar before and after HL treatment, indicating that energy spillover from PSII to PSI did not take place during photoinhibition. This conclusion is supported by the similarity of q_I amplitude and kinetics in the *stt7-9* and ΔPSI strains (fig. S4).

To verify whether q_I involves the LHCs via an aggregation-independent mechanism, we examined three strains with reduced antenna content (fig. S5). Mutants affected in the import of the LHCs to the chloroplast or deficient in Chl *b* were used. In all these mutants, the relation between q_I and photodamage was similar to that of the reference strains (fig. S5) when accounting for the reduced PSII cross section. This supports the conclusion that LHCs are not the site of q_I.

We observed that despite the initial absence of LHCSR3 in the cells, expression of this q_E-inducing protein took place during HL treatment (fig. S5). To verify whether it could contribute to q_I, we analyzed the *stt7-9 npq4* double mutant, where LHCSR3 is knocked out (*9*). In this mutant, the q_I amplitude and kinetics remained comparable to the control, excluding the option of LHCSR3-dependent q_I (fig. S5).

The results described above suggest that q_I occurs within the PSII core. This is supported by the analysis of the ΔPSII mutant, which shows far less quenching and slower induction kinetics than the control and the ΔPSI mutant (fig. S4; see also Discussion).

Loss of q_I is light independent and does not require chloroplast translation

Next, we investigated the dependence of the quenching from PSII repair by measuring the stability of q_I in the long time scale in the absence of D1 resynthesis. We also extended the study beyond the *stt7-9* mutant and included three wild-type (WT) strains with distant genetic backgrounds (*40*): CC-124, CC-1009, and CC-1690. The influence of state transitions on fluorescence signals during photoinhibitory treatment was accounted for (see fig. S3 for details).

Following photoinhibition, all tested strains developed q_I. While the maximal amplitude varied between 1 and 1.4, q_I reached a maximum and then strongly decreased ~1 hour after the onset of HL treatment in all strains (Fig. 2A; see fig. S3E for the *stt7-9* strain data). Unexpectedly, this decrease proceeded in the presence of lincomycin, indicating that it was not related to de novo PSII subunit synthesis (Fig. 2B) or to a recovery of the PSII function, as also indicated by the fact that F_V/F_M did not change during the fluorescence recovery period (Fig. 2C). Furthermore, the loss of quenching occurred already during the HL period. Neither the duration of the HL treatment (after reaching the peak of q_I amplitude) nor whether it was followed by a dark period or low-light treatment had a substantial influence on the loss of q_I (fig. S6). Together, these results indicate that a slow, light-independent process, which does not require active chloroplast translation, governs most of the q_I loss.

Loss of q_I relies on PSII proteolysis by FtsH

We hypothesized that the slow, light-independent q_I loss is due to the degradation of PSII core subunits within which q_I occurs (Fig. 2B). To test that, we measured q_I in *ftsh1* mutants, where the major metalloprotease involved in PSII degradation (*41*–*43*) is inactive (*ftsh1-1*) or present in a low amount (*ftsh1-3*). The amplitude and kinetics of q_I induction in the *ftsh1* mutants closely followed those of the reference WT strain (Fig. 3A and fig. S7). However, the mutants remained quenched for a far longer time (Fig. 3A and fig. S7) than the controls. This behavior was *ftsh1* dependent, as demonstrated by the fact that the complemented strains showed q_I loss (Fig. 3A and fig. S7).

To be able to correlate the protein degradation with fluorescence changes in the absence of state transitions influence on the emission, we constructed the *stt7-9 ftsh1-1* double mutant (fig. S8). As shown in Fig. 3B, both *stt7-9* and *stt7-9 ftsh1-1* strains lost full-length D1 protein upon HL treatment, with the initial cleavage being slower in the double mutant (see quantification of the relative amounts of PSII core proteins in fig. S9). As observed before (*42*), the *stt7-9 ftsh1-1*

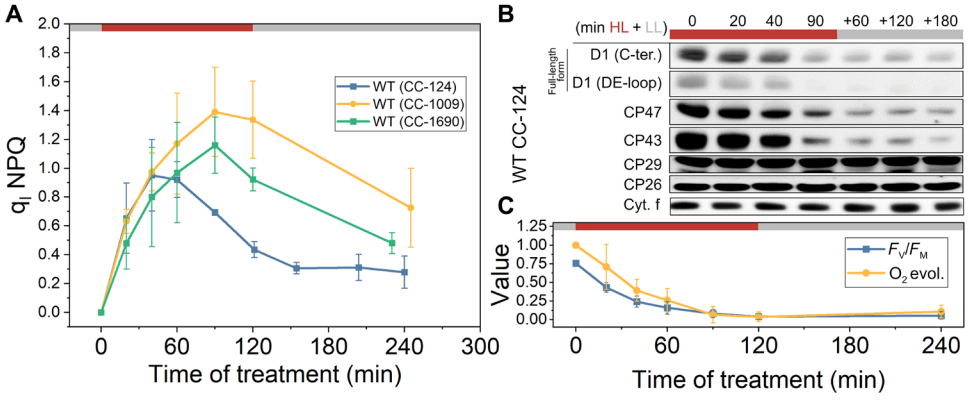

Fig. 2. q_I is transient, and its loss is independent of PSII repair. All experiments shown were performed in the presence of lincomycin, which inhibits chloroplast translation and D1 resynthesis. Red boxes, HL illumination (1500 μmol photons m^{-2} s^{-1}); gray boxes, low-light (LL) period (15 μmol photons m^{-2} s^{-1}). (**A**) Development of q_I in three WT strains (CC-1009 and CC-1690: $n = 3$; CC-124: $n = 6$) upon exposure of the cells to HL followed by LL. (**B**) Immunoblotting with antibodies against selected PSII subunits during HL and LL exposure in the CC-124 WT strain. (**C**) PSII activity in WT (CC-124) during HL treatment followed by an LL period, measured using fluorescence (F_V/F_M) and O_2 evolution capacity. $n = 3$.

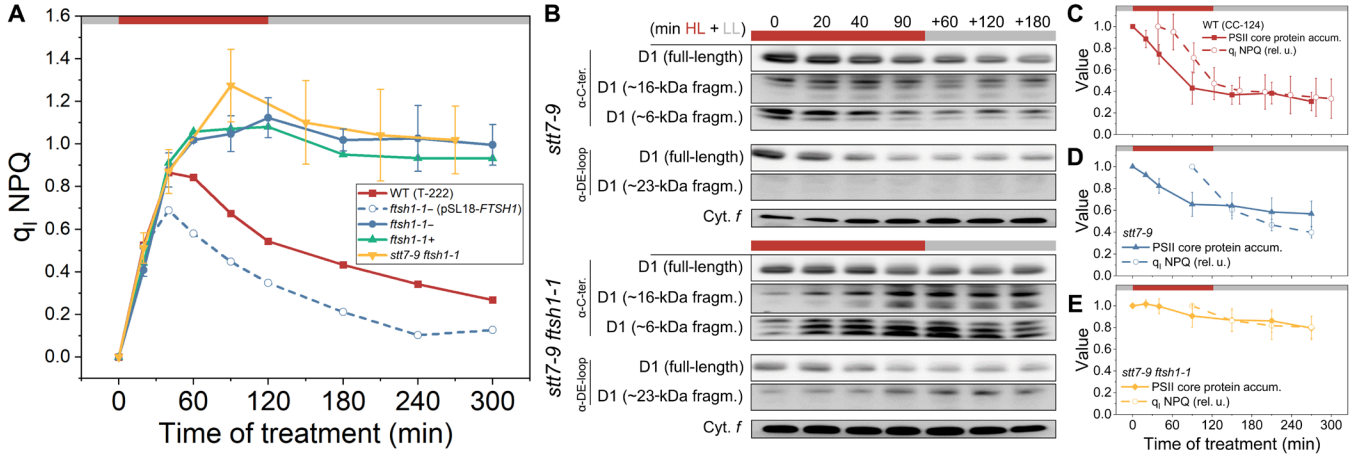

Fig. 3. q_I quenching loss is due to PSII core proteolysis by FtsH. All experiments shown were performed in the presence of lincomycin, which inhibits chloroplast translation and D1 resynthesis. Red boxes, HL illumination (1500 μmol photons m^{-2} s^{-1}); gray boxes, LL period (15 μmol photons m^{-2} s^{-1}). (**A**) q_I quenching behavior upon photoinhibition. WT (T-222) is the parental strain of the *ftsh1-1* mutant. Two separate clones of the *ftsh1-1* allele are shown together with the *ftsh1-1*:pSL1 FTSH1 complemented strain and the double mutant *stt7-9 ftsh1-1*. See also fig. S7 for the *ftsh1-3* allele. (**B**) D1 degradation time course in *stt7-9* and *stt7-9 ftsh1-1* strains, followed by immunoblotting. One representative biological replica is shown; relative accumulation of cytochrome *f* is not affected by photoinhibition and was used as a loading control. (**C**) PSII RC protein loss [average of relative signal from three antibodies (α-DE loop and α-C-ter. of D1; α-CP47); see fig. S9 for raw quantification data], $n = 1$, and relative q_I NPQ, $n = 6$, in WT (CC-124). (**D**) PSII RC protein loss, $n = 3$, and relative q_I NPQ, $n = 3$, in *stt7-9* strain. (**E**) PSII RC protein loss, $n = 3$, and relative q_I NPQ, $n = 3$, *stt7-9 ftsh1-1* strain.

strain accumulated short fragments of D1 (Fig. 3B), due to the absence of FtsH-mediated exoproteolytic degradation. In line with these observations, blue-native polyacrylamide gel electrophoresis (BN-PAGE) showed that, during photoinhibition, the amount of the small PSII supercomplexes decreased far more in *stt7-9* than in the double mutant (fig. S10).

Together, these experiments demonstrate the impaired PSII RC complex proteolysis in the *ftsh1* background. Overall, the loss of q_I showed correlation with the PSII protein degradation across *stt9* and *stt7-9 ftsh1-1* strains (as well as in the WT), although it exhibited a lag with regard to proteolysis (Fig. 3, C to E). These observations indicate that loss of intact PSII core leads to the loss of quenching (Fig. 3, C to E). The observed lag in quenching loss could potentially be explained in the context of energetic connectivity in the thylakoids: The decrease of quenching due to PSII degradation is temporarily limited by the presence of quenching sites in nearby PSIIs (see the "Photoinhibited PSII RCs are heterogeneous" section for details).

The location of the q_I site in the photoinhibited PSII core was finally confirmed by the ΔPSII mutant, in which no loss of q_I was observed either in HL or in low light (LL), indicating that the slow quenching observed in this strain (fig. S4) has a different origin, and resembled what was observed before in cells lacking both photosystems exposed to HL (*44*).

Formation of q_I site requires oxygen

To understand the sequence of events upon photoinhibition, we focused on the initial kinetics of q_I and other functional and biochemical observables. As shown in Fig. 4A, loss of fluorescence (F_M) was by far the fastest event upon HL treatment ($t_{1/2}$ of ~15 min). F_V/F_M decreased slower ($t_{1/2}$ of ~30 min), but as expected, it showed good correlation with the decrease of oxygen evolution. Crucially, the degradation of PSII RC proteins was substantially slower than the changes in fluorescence and oxygen evolution (Fig. 4A), in line with previous reports (*17*). These results substantiate the above hypothesis that protein degradation is related to the loss of q_I rather than to its induction and highlight that q_I is one of the earliest events upon photoinhibition.

The fact that the formation of the quenching site within the core of PSII precedes D1 cleavage leaves several options regarding the quenching mechanism, including nonphotochemical energy dissipation and charge separation–based quenching. It was recently shown that protein oxidation events take place early upon photoinhibition (*15*) and that they can induce quenching in pigment-protein complexes (*45*); furthermore, it was observed that oxygen influences the F_M level during photoinhibition (*46*). We thus investigated whether oxygen is necessary for (i) the quenching itself or (ii) for the formation of the q_I site. To test the first hypothesis, we induced anoxia in photoinhibited cells. In this case, the quenching capacity remained unchanged, demonstrating that O_2 is not necessary for energy dissipation once q_I site is formed (fig. S11). In addition, this indicates that reducing conditions, particularly affecting the PSII electron acceptor pool, are not preventing the quenching from taking place. To test whether oxygen is necessary for the formation of the q_I site, we conducted photoinhibitory treatment in anoxia. Addition of DCMU was necessary to prevent O_2 evolution by PSII. The presence of this inhibitor under oxic conditions had a minor influence on the rate of q_I formation (Fig. 4B), likely due to a change of Q_A energetics upon DCMU binding (*47*), but did not affect the amplitude of HL-induced quenching. However, upon anoxic photoinhibition, the q_I amplitude was strongly reduced (Fig. 4B) and the PSII closure was slower (fig. S12) than at ambient O_2 concentration. This strongly suggests that presence of oxygen (ambient or nascent on the PSII donor side) is required for the formation of the quenching site. We interpret this as a ROS-mediated oxidation of a specific pigment within the PSII RC, leading to a formation of the quenching site (Fig. 4B). In conclusion, the oxygen dependence of q_I site formation indicates that quenching arises by the inactivation of PSII RC, likely through

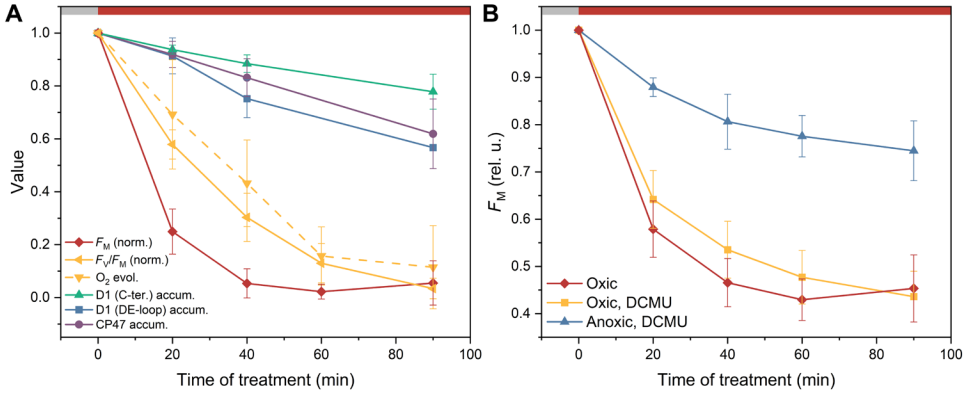

Fig. 4. q_I site formation is rapid and requires the presence of oxygen. All experiments were performed in the presence of lincomycin, which inhibits chloroplast translation and D1 resynthesis, in the *stt7-9* strain. Red boxes, HL illumination (1500 μmol photons m^{-2} s^{-1}); gray boxes, LL period (15 μmol photons m^{-2} s^{-1}). (**A**) Changes in photosynthetic parameters and relative protein accumulation upon photoinhibition. F_M, F_V/F_M, and oxygen evolution changes, $n = 11$; PSII RC protein accumulation (rel.), $n = 3$. F_M was normalized between its maximal and minimal values and F_V/F_M to its maximum. (**B**) Fluorescence quenching under anoxic conditions. $n = 3$ (DCMU; anoxic, DCMU) and $n = 11$ (oxic conditions).

an RC chlorophyll oxidation. These observations support a charge recombination–based formation of the q_I site.

Photoinhibited PSII RCs are heterogeneous

The induction and loss of photoinhibition-related quenching is a complex process that occurs on a minute to hour time scale. During HL exposure, changes in fluorescence parameters, such as F_M and F_V/F_M, occur faster than the degradation of the RC proteins (Figs. 2 to 4). Notably, the decrease of F_M precedes the loss of PSII activity (F_V/F_M). Moreover, during the dark period following HL exposure, there is a loss of q_I correlating with the D1 proteolysis after a lag phase and without a corresponding change in F_V/F_M (Figs. 2 and 3, C to E). To understand these observations in the context of a structure-based model of light harvesting (Fig. 5, A to C), we hypothesized that there are two distinct types of photoinhibited RCs, both unable to perform photochemistry: (i) "quenching" centers, which exhibit q_I capacity, and (ii) "broken" centers, which do not. All together, our minimal model contains active RCs that are either "open" (F_0) or "closed" (F_M) and inactive RCs that are either quenching or broken (Fig. 5D).

We built a kinetic model to describe the slow (minute to hour) processes that convert RCs between the four types (Fig. 5E). We explain the decrease of F_M following HL exposure by assuming that there is a light-dependent reaction that converts active RCs to quenching RCs. We assume that the rate of q_I site formation is equivalent in both the *stt7-9* and the double mutant *stt7-9 ftsh1-1* (see Supplementary Text for other models). In the absence of D1 resynthesis, the loss of fluorescence quenching suggested a proteolytic degradation of quenching RC complexes (Fig. 3), which we propose forms broken RCs. The *ftsh1* mutation decreases the proteolytic activity and thereby reduces the conversion rate of quenching into broken complexes. Thus, our kinetic model has three parameters to describe the time evolution of RC populations: the rate from active to quenching ("q_I site formation") and the rate from quenching to broken ("degradation of quenching centers"), which has two possible values depending on the presence/absence of FtsH.

We connected the evolving RC populations to the fluorescence observables using a structure-based model of excitation energy transport on a 40,000 nm^2 patch of the appressed thylakoid membrane (Fig. 5A) (*4*, *48*, *49*). Excitation energy transfer between chlorophyll domains was described using generalized Forster theory [Fig. 5, B and C; see Materials and Methods for details; (*50*)], and charge separation at active RCs [Fig. 5C; (*49*)] was described using previously established parameters [see Materials and Methods and (*48*, *49*) for details]. The rate of excitation dissipation (k_{qI}) at quenching RCs was treated as a free parameter because of the absence of any experimental bounds. For a given population of open, closed, quenching, and broken centers, we constructed the ensemble average fluorescence values using 20 realizations of different random assignments of PSII complexes to each group. The simulated ensemble average was then compared to the experimental fluorescence measurements.

We constructed the best-fit model for photoinhibition by simultaneously minimizing the error compared to the steady-state fluorescence measurements for both the *stt7-9* and *stt7-9 ftsh1-1* mutants (Fig. 5E). For *stt7-9* at 0-min HL, the excitation energy transfer model successfully reproduces both steady-state F_V/F_M (sim., 0.8; exp., 0.82) and time-resolved fluorescence measurements (Fig. 5N). The *stt7-9 ftsh1-1* double mutant at 0-min HL has a substantially shorter F_M fluorescence lifetime than the *stt7-9* strain, which we assume arises from previous exposure to the growth light and slow PSII repair (*41*, *42*). We fit the short F_M fluorescence lifetime to a residual mixture of broken (34%) and quenching (6%) RCs (Fig. 5P), which also reproduces the steady-state decrease in F_V/F_M value (sim., 0.65; exp., 0.67) at 0-min HL.

The best-fit kinetic model has a q_I quenching rate (k_{qI}) of 0.1 ps^{-1}. A single rate of q_I site formation (0.027 min^{-1}) successfully describes the onset of quenching in both strains and shows a rate of quenching center degradation that is two orders of magnitude slower in *stt7-9 ftsh1-1* compared to *stt7-9* (Fig. 5, E to M). The model supports the hypothesis that irreversible closing of RCs and q_I site formation occur simultaneously, in line with the proposed mechanism in which the quencher formation is the result of ROS-mediated damage of a PSII RC pigment. Overall, the photoinhibition model proposed here not only correctly simulates the steady-state fluorescence in both strains with a minimal kinetic scheme but also reproduces the trends of protein degradation (Fig. 5, O and Q). The latter thus suggests that the proteolytic degradation of RC complexes is sufficient and necessary to abolish q_I and that the lag observed in

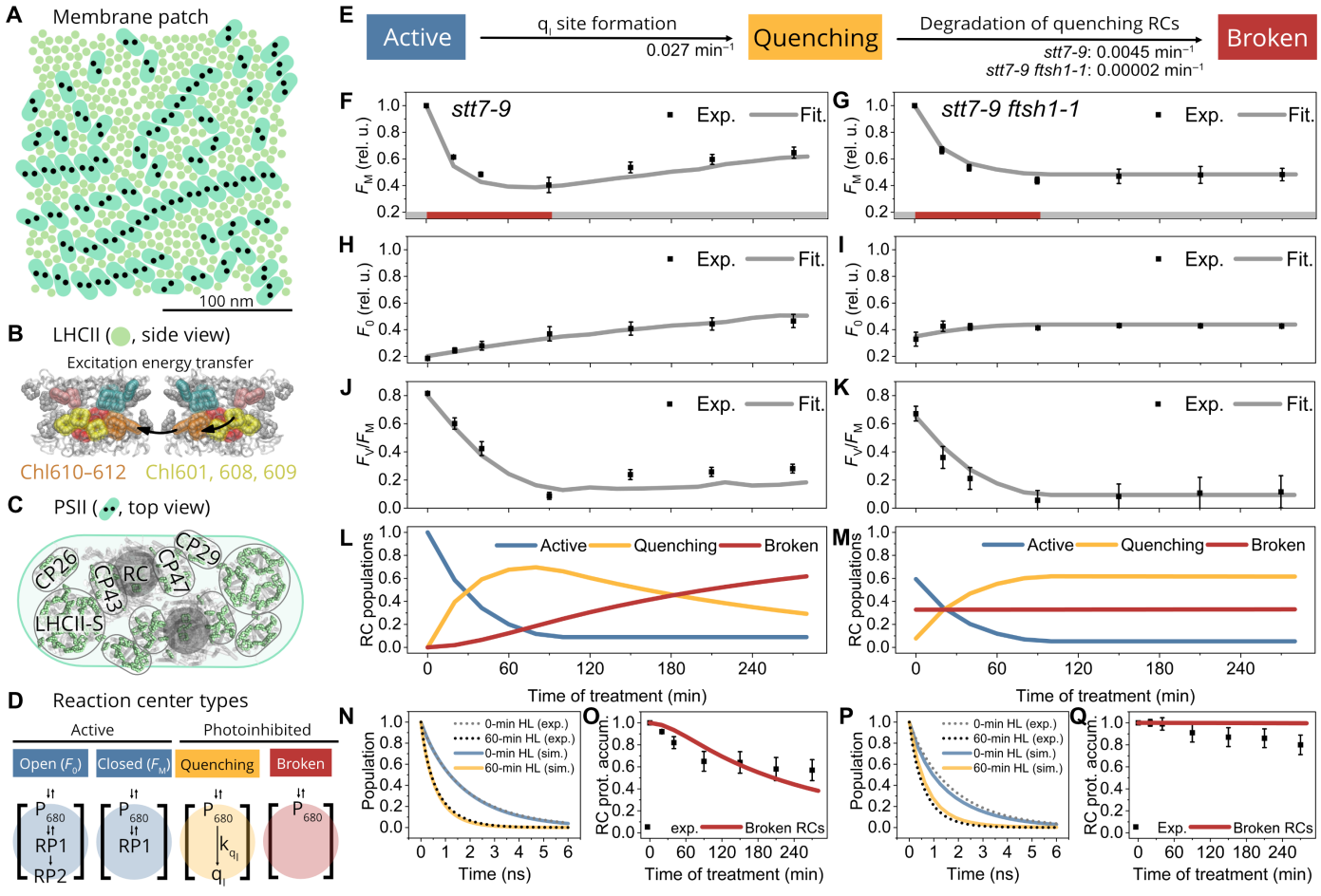

Fig. 5. Heterogeneity of photoinhibition revealed through membrane-scale structure-function modeling. The model represents an appressed region of the thylakoid membrane containing PSII-LHCII supercomplexes. All experimental points are means ± SD; $n = 3$; modeled data are shown in thick lines. Red boxes, HL illumination; gray boxes, LL period. (**A**) Organization of photosynthetic complexes in the membrane patch used for the modeling. (**B**) Coarse graining of pigment domains in LHCII. Fluorescence resonance energy transfer between the domains within an LHCII and between adjacent antennae is shown with arrows. (**C**) PSII supercomplex structure used in the model. (**D**) Types of RCs used in modeling and their characteristics. "Open RCs" have an initial reversible charge separation (RP1) and a slower irreversible charge separation (RP2). "Closed RCs" have a slower rate of initial charge separation (RP1) with a faster rate of recombination and are not able to stably charge separate. "Quenching RCs" have no rate of charge separation but have a separate q_I NPQ mechanism with a rate k_{qI}. "Broken RCs" have no charge separation or quenching pathways. (**E**) Kinetic model of photoinhibition used for the modeling. The rates were obtained by fitting the data from (F) to (K). (**F** and **G**) Experimental and modeled fluorescence yields during photoinhibition when all RCs are closed (F_M state). (**H** and **I**) Like (F) and (G) but when all active RCs are open (F_o state). (**J** and **K**) Experimental and modeled changes in the F_V/F_M parameter during photoinhibition. (**L** and **M**) Modeled kinetics of the populations of active, quenching, and broken RCs during photoinhibition. (**N** and **P**) Experimental (dotted line) and modeled (continuous line) time-resolved fluorescence traces of PSII-related components. (**O** and **Q**) Experimental and modeled changes in the relative accumulation of full-length PSII RC proteins throughout. (F, H, J, L, N, and O) *stt7-9* strain. (G, I, K, M, P, and Q) *stt7-9 ftsh1-1* strain.

Fig. 3 (D and E) could be simply interpreted as a result of energetic connectivity. We lastly confirmed the self-consistency of this model by reproducing fluorescence lifetime measurements after 60-min HL treatment (Fig. 5, N and P).

Here, we have demonstrated that a minimal model containing two types of photoinhibited RCs and three kinetic rates can reproduce both fluorescence measurements reporting on the ultrafast process of light harvesting and immunoblotting data describing protein degradation on the minute time scale (see Supplementary Text and fig. S19 for more details). Therefore, the model links kinetics spanning 14 orders of magnitude and provides a predictive framework for understanding a broad range of photoinhibition-related events in vivo. Crucially, this model is parsimonious, successfully accounting for the q_I formation and RC closure upon photodamage, without a necessity of evoking two quenching sites and mechanisms proposed earlier (*28*, *30*).

DISCUSSION

It is of little surprise that photoinhibition, damaging one of the most complex enzymes in biology, is itself a complicated process. Understanding PSII damage and repair is crucial because of the importance of photoinhibition in crop and aquatic photosynthesis (*18*, *21*, *22*, *51*). However, the molecular nature of q_I has been rarely addressed in the literature (*27*–*30*). In this work, we have simultaneously analyzed several aspects of this process, which will be discussed here to provide a picture of the formation and relaxation of q_I (Fig. 7).

Connectivity between PSII complexes and its influence on F_V/F_M

Historically, oxygen evolution, spectroscopy, and biochemical measurements were used to quantify PSII damage (*19*, *52*, *53*). In particular, changes in the photochemical yield of PSII assessed through fluorescence measurements (e.g., F_V/F_M) are commonly used to quantify photoinhibition. However, the decrease of F_V/F_M is not linearly related to the amount of broken PSIIs, but rather, it describes the global maximal photochemistry. This is due to the energetic connectivity, which results in an increase of the antenna size of the active centers by pigments belonging to the photoinhibited complexes (up to 50 nm apart) (*48*). Our simulations indicate that the formation of damaged centers is faster than the decrease of F_V/F_M and slower than the apparent F_M changes (Fig. 6), in line with previous experiments (*54*).

Mechanisms of photoinhibition and potential heterogeneity of damage

At least two mechanisms for photoinhibition have been discussed in the literature (*19*): a donor side mechanism targeting initially the OEC and occurring in blue and UV light (*19*, *24*, *25*); and an RC-based mechanism involving photochemistry and ROS, but occurring also in anoxia (*23*, *55*).

Our results agree with a combination of the two mechanisms (*23*). Under our light conditions (fig. S14), OEC damage and RC impairment take place in parallel rather than sequentially, in agreement with a previous proposal (*54*, *56*). The oxygen dependence of q_I formation (Fig. 4) and the slower F_V/F_M decrease in anoxia (fig. S12) suggest that, in our experimental conditions, the oxidative RC damage is faster than the donor side photoinhibition but that, in the absence of O_2, the latter still takes place. Crucially, photoinhibition linearly correlates with light intensity (*19*) (fig. S13) and RC closure takes place simultaneously with the q_I site formation (Fig. 5). We therefore consider that the oxidative damage involves modifications in the PSII RC vicinity through in situ singlet oxygen sensitization proceeding by PSII charge recombination. As demonstrated by Rehman *et al.* (*26*), $^1O_2$ formation by $^3P_{680}$ (a by-product of charge recombination) linearly correlates with light intensity, in line with this hypothesis ((*20*), although we note that singlet oxygen formation can proceed in vitro even in the absence of PSII RC (*55*)).

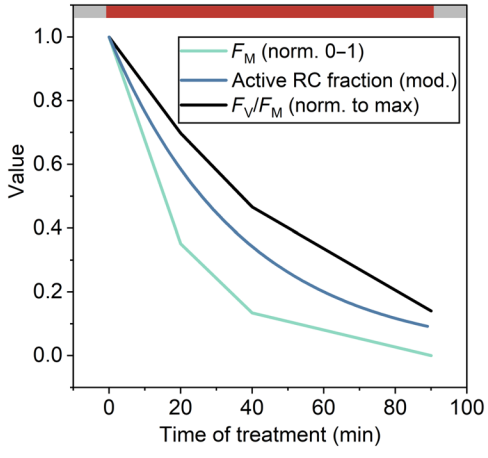

Fig. 6. Kinetics of fluorescence changes and the variation in active RC concentration upon photoinhibition. Concentration of the active RCs obtained from membrane-scale simulations. Means of fluorescence measurements in the *stt7-9* strain are depicted, $n = 3$. F_V/F_M was normalized to its maximal value and F_M between 0 and 1. Red box, HL illumination (1500 μmol photons m^{-2} s^{-1}); gray boxes, LL period (15 μmol photons m^{-2} s^{-1}).

The parallel model implies that the two modes of photoinhibition can be separated. An argument in agreement with that is provided by our experiment under anoxic conditions where we observed the appearance of a light-induced quenching of small amplitude (fig. S11) in HL-treated samples. This quenching hints at a capacity of P_{680}^+ formation due to the dysfunctional donor side and simultaneously to a partially active acceptor side, thanks to the absence of oxygen sensitization. The dependence of photoinhibition and fluorescence parameters on light color supports the same conclusion (*54*).

The kinetic model of photoinhibition (Fig. 5) provides insights into the heterogeneity of PSII RC composition during HL treatment. It demonstrates that even in the case of a null F_V/F_M value, a combination of quenching and broken RCs is present in the thylakoids (Fig. 5, L and M). Nonetheless, our model supports a homogeneous damage mechanism, with a simple conversion of active RCs to quenchers, followed by their degradation and loss of q_I sites (but see also Supplementary Text and fig. S19). This finding succeeds in describing the kinetically different behavior between F_M and F_V/F_M. In addition, the close match between the appearance of broken centers and PSII core subunit degradation suggests that the latter process abolishes the quenching capacity in vivo.

q_I quenching site and mechanism

An intrinsic regulation of the rate of $^1O_2$ production is built into the PSII, decreasing the rate of PSII charge recombination (*7*, *26*). It depends on the presence of functional donor and acceptor sides of PSII (*6*, *7*). The midpoint redox potential (E_m) of the Q_A quinone increases by around 115 mV when OEC is impaired and by 75 mV in the absence of the HCO_3^- between Q_A and Q_B. As a consequence, direct recombination between P_{680}^+/Q_A^- (or Tyr_Z^+/Q_A^-) is favored over a repopulation of the P_{680}^* state. Such charge recombination could, in principle, also constitute the q_I mechanism; when the donor side of PSII is impaired upon photoinhibition, radiationless recombination would result in a quenching of fluorescence (*27*). Our experiments, however, show that it is an unlikely scenario, as the redox state of Q_A before fluorescence measurement plays no role in the extent of quenching observed after the q_I site is established (Q_A state in regular, oxic conditions; Q_A^- state in the presence of DCMU, in anoxia, and upon actinic light illumination; fig. S11B). We nonetheless note here that, if the E_m of Pheo was also substantially increased by PSII donor side impairment, then similar recombination-based quenching ($P_{680}^+/Pheo^-$) could still take place and would be less dependent on oxygen tension.

Conversely, oxygen presence was necessary to form the q_I site within the PSII RC. The formation of $^1O_2$ is well established upon photoinhibition, and ROS have been shown to damage the protein scaffold (*15*). Pigment oxidation also results in a shortening of chlorophyll excited-state lifetime (*45*). Last, singlet oxygen concentration increases linearly with light intensity, as does the rate of q_I formation (fig. S13); moreover, this rate decreases slightly upon oxic photoinhibition in the presence of DCMU, which increases Q_A E_m, therefore reducing the recombination-induced $^1O_2$ production Fig. 4B (*47*). Thus, a hypothesis where $^1O_2$ formed via $^3P_{680}$ directly oxidizes one of the RC pigments, impairing charge separation capacity and forming the q_I site, is consistent with all the data. This interpretation

is lastly supported by recent mutagenesis results suggesting that Chl_{D1} itself is the primary damage site of $^1O_2$-mediated oxidation (*57*), as well as remains valid if a double Q_A reduction to Q_AH_2 takes place in anoxia. We therefore propose that photooxidized Chl_{D1} is the primary site of q_I quenching.

Is photoinhibition photoprotective?

Quenching is often associated with photoprotection. In the case of photoinhibition-related quenching, the situation is more complex, as damage is a prerequisite for quenching. The linear dependence of photoinhibition on light intensity and first-order kinetics of PSII function loss [see discussion in (*19*, *58*) and references therein] is supported both by the donor side damage, mediated by the direct light absorption by the OEC and through recombination-induced $^1O_2$ formation (*26*). The former damage cannot be prevented by quenching but only by photoprotective adaptations such as screens on the leaf surface (*59*). This interpretation becomes slightly more nuanced in the scope of the hybrid photoinhibition model (*19*, *23*): The donor side mechanism might be inevitable, but the oxidative RC impairment could potentially be alleviated by decreasing the number of excitations used for charge separation. However, it is important to stress that F_V/F_M measurements do not distinguish between these two mechanisms (fig. S12) and that using quenching as the observable might be beneficial in this regard (Fig. 4).

Ultimately, while PSII photodamage studies are invariably done in the absence of D1 resynthesis, under natural conditions, limiting ROS production protects the repair machinery (*60*) and alleviates damage in the steady state (*10*, *61*). Hence, q_I can positively influence the recovery from photoinhibition, even if not substantially preventing PSII damage (*62*, *63*). In particular, PSII assembly provides cues that agree with the necessity of prevention of PSII RC oxidation and of a decrease of ROS formation. The abovementioned changes in Q_A E_m were recently shown to dampen the singlet oxygen production before PSII became fully assembled (*7*, *64*).

Crucially, however, by damaging the PSII RC complex, photoinhibition prevents the formation of long-lived quenching in LHCII (fig. S4), the appearance of which indicates that oxygen sensitization can lead to irreversible damage of antenna pigments (fig. S4). We highlight that this antenna quenching was almost absent in the presence of PSII, as demonstrated by the almost complete FtsH-dependent loss of q_I (Figs. 2 and 3). The stability of quenching in HL in the absence of PSII core (*44*) suggests that it is difficult to eliminate this energy dissipation, which can be detrimental to photosynthetic efficiency following HL exposure [as suggested in the case of too-slowly-relaxing q_E (*65*)]. This, in turn, underscores that locating q_I in the replaceable PSII RC is another feat of PSII, whose design and function do not cease to surprise (*6*, *64*).

Potential mechanisms of D1 damage

Whether offering substantial photoprotection or not, quenching centers are damaged and thus need to be repaired (*52*, *53*, *66*, *67*), starting with the degradation of the D1 protein. The mechanism of D1 proteolysis is debated, with at least three known processes involved: (i) Passive cleavage of D1 was observed upon HL treatment in vitro (*68*, *69*), likely involving protein radicals formed upon photoinhibition (*15*, *70*) or even by P_{680}^+-mediated oxidation. This mechanism yields similar D1 degradation fragments as photoinhibition in vivo, which is presumed to proceed through (ii) Deg-mediated endoproteolysis (*71*–*73*), followed by FtsH-mediated processing of D1 fragments (*42*). (iii) Direct degradation of D1 by FtsH was also observed (*52*), in line with our data (fig. S9). However, the light-dependent change in the rate of full-length RC protein degradation (Fig. 3 and fig. S9) suggests that a combination of these mechanisms takes place in living cells.

The luminal subunits of PSII [PsbO/P/Q; (*3*)] shield the D1 peptide from proteolysis by DEG. Their dissociation was shown to correlate with D1 cleavage (*74*, *75*), and it could constitute the rate-limiting step of degradation. On the other hand, the relatively slow D1 cleavage might be due to the limited capacity of PSII complexes to migrate to the nonappressed regions of the thylakoids. The repair cycle was proposed to take place in the stroma lamellae or grana margins, to account for the accessibility of damaged D1 to the bulky stroma-exposed subunits of FtsH (*52*, *71*, *75*, *76*). In such case, the *stt7-9* effect slowing down RC peptide degradation could be due to the impairment in membrane fluidity and movement of damaged PSII RCs.

We have demonstrated that the quenching is lost because of proteolysis (Figs. 3 and 5), and we envisage two mechanisms that can account for that. On the one hand, initial cleavage of D1 might result in a loss of q_I capacity. The microenvironment of the hypothesized oxidized RC pigment, likely Chl_{D1}, could influence q_I or the excitation energy transfer to this site. Another possibility is that the RC complexes with cleaved D1 still remain assembled (at least a fraction of them does, as shown in fig. S10) and retain the ability to perform quenching because only complete degradation of the RC core removes the q_I site (see Fig. 7, inner polar plot). However, the quantification of the latter process is difficult because of the complexity of the solubilization of membrane complexes containing cleaved peptides. If the RC complex degradation rapidly follows the initial cleavage of D1, then the distinction between these two processes might prove difficult.

Last, while we did observe degradation of CP47, this was likely a result of the absence of de novo D1 synthesis (blocked consistently with lincomycin) and thus its assembly partner (*77*). Of all RC proteins, D1 has, by far, the fastest turnover (*16*, *67*, *78*), confirming that, in many cases, replacement of D1 is the only requirement for PSII repair after photodamage.

The experiments in *ftsh1* mutant background provide another advantage in our understanding of photoinhibition-related fluorescence decrease. The long-term stability of the quenching in the absence of degradation (Figs. 3 and 5) strongly suggests that q_I is the sole quenching mechanism observed (Fig. 1). This is preserved despite the changes in the ultrastructure of thylakoids changes upon photoinhibition (*75*).

In this work, we used integrated approaches to study photoinhibition and the related q_I quenching in vivo. A consistent description of all observables across multiple time scales was achieved using a modeling approach in the context of energetic connectivity. We were able to exclude a number of potential quenching sites thanks to spectrally and time-resolved fluorescence measurements and the use of multiple mutants. We propose that the q_I site is formed by a singlet oxygen–mediated attack on one of the PSII RC pigments, likely Chl_{D1}, simultaneously closing the RC and forming a quenching site. This process at once decreases the F_M fluorescence level and raises F_0. Quenching RCs are then lost through FtsH-mediated degradation of PSII. This unified model does not require separate processes to account for the contrasting kinetics of steady-state fluorescence parameters, nor a heterogeneity in quenchers. Our model

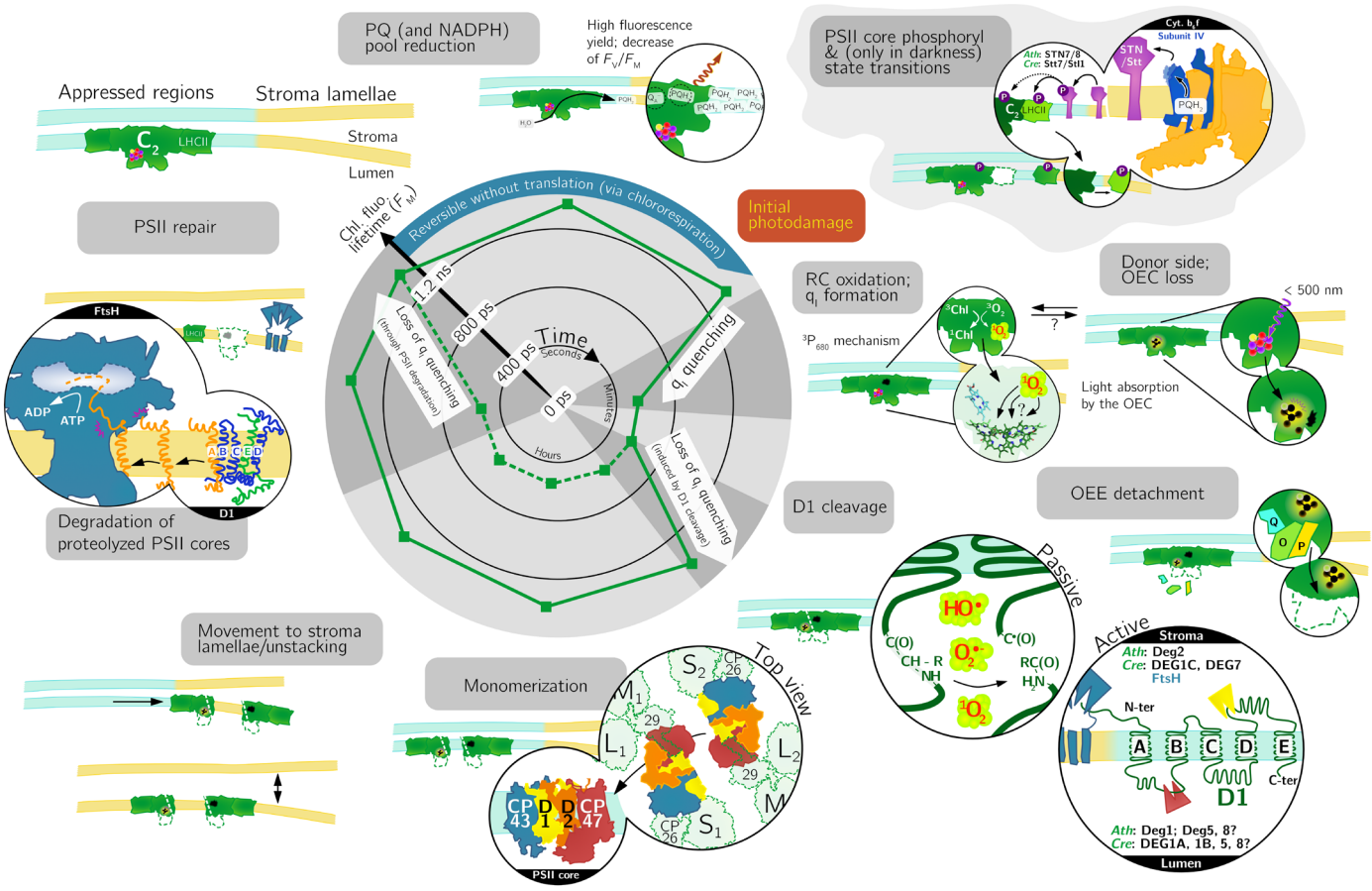

Fig. 7. Schematic model of the induction and relaxation of q_I upon photoinhibition. Initial photodamage to PSII supercomplex (core dimer, C_2; antenna, LHCII) can be described by two independent mechanisms: light-induced ROS formation and oxidation of PSII subunits and pigments, as well as the direct OEC damage (*19*). q_I (inner polar plot of the average fluorescence lifetime in vivo), established with a halftime of ~15 min, is concomitant with photodamage. The loss of quenching is either a direct result of D1 cleavage (continuous line) or FtsH-mediated degradation of RC complexes (dashed line). Following D1 cut (potentially preceded by detachment of PsbO/P/Q subunits from the complex), the PSII monomerizes but remains at least partly assembled despite the endoproteolysis of its RC protein. It then translocates to non-appressed regions of the thylakoids (or else the appressed regions unstack). Transmembrane thylakoid FtsH protease degrades the D1 protein and the PSII RC complex. PSII repair with de novo synthesis of at least D1 subunit takes place to reestablish the initial state. NADPH, reduced form of nicotinamide adenine dinucleotide phosphate; ATP, adenosine triphosphate; ADP, adenosine diphosphate; OEE, oxygen-evolving enhancer.

of photoinhibition where donor-side and oxidative RC damage take place independently, with only the latter forming a quenching site, will help to understand this complicated process from a novel perspective.

MATERIALS AND METHODS

Experimental design

To study photoinhibition-related quenching in vivo, we used the model green alga *C. reinhardtii*. The cells were grown under LL, heterotrophic conditions. Unless stated otherwise, *stt7-9* strain was used. As a result, the changes in fluorescence were devoid of NPQ or influence of state transitions, and they were further shown not to stem from pigment loss thanks to time-resolved emission measurements. Thus, the q_I quenching was isolated in vivo throughout the study.

WT strains [CC-1009 and CC-1690 (*40*)] and *tla3*− (*79*) were obtained from Chlamydomonas Resource Center. Genetic cross between *stt7-9*+ strain (*36*) and *ftsh1-1*− (*42*) was performed, yielding the *stt7-9 ftsh1-1* double mutant (fig. S8). Other strains used [BF4 and *pg27* (*80*), *ftsh1-3* (*42*), ΔPSII *Fud7.S2*+ (*81*), and ΔPSI *F14.1*− (*82*)] were acquired from ChlamyStation (chlamystation.free.fr).

All strains were grown under mixotrophic conditions in shaking glass flasks (tris-acetate-phosphate medium, 25°C, continuous 15 μmol photons m^{-2} s^{-1} light-emitting diode (LED) light illumination from the bottom; see fig. S15 for the growth light spectrum). When in early-log phase (1 million to 2 million cells/ml), the cells were spun down at 3000 rpm for 5 min and resuspended in approximately one-fifth volume of tris-phosphate medium (Min) without reduced carbon source. $NaHCO_3$ (1 mM) was systematically added to replete the bicarbonate binding site in PSII and lock its redox tuning (*6*). Concentrated cells were then put back for recovery to their growth chamber for at least 2 hours before the measurements.

For photoinhibitory treatment, concentrated cultures were exposed to HL (1500 μmol photons m^{-2} s^{-1}; same light source as for growth; fig. S15) in the presence of chloroplast translation inhibitor lincomycin (1.2 mM). The samples from different time points after HL treatment were then dark-adapted (15 min) before each

measurement unless stated otherwise (figs. S1B and S3F). For anoxic photoinhibitory treatment under the same conditions, but starting from at least 30 min before HL exposure, the cultures were flushed with a mix of 1% (v/v) CO_2 in N_2, and 10 μM DCMU [3-(3,4-dichlorophenyl)-1,1-dimethylurea] was added before photoinhibition. Anoxia after regular photoinhibitory treatment was achieved by an addition of glucose (20 mM) and glucose oxidase (type II from *Aspergillus niger*; 50 U/ml) to the cuvette with algae shortly before the measurement. In both cases of anoxia, saturating light was used to fully reduce Q_A.

Spectroscopy

Fluorescence and transient absorption measurements were done using the JTS-10 apparatus (BioLogic). In fluorescence mode, detecting white LED flashes were filtered through a narrow interference filter [520 nm, 10-nm full width at half maximum (FWHM), and 10 mm] and triggered within short (~300 μs) dark periods of actinic illumination ("dark pulse" mode). The detection was done with a long-pass filter (cutoff at 670 nm, 10 mm, Schott). Actinic light was provided from both sides of the cuvette in a custom-built holder (JBeamBio) and was set to a subsaturating value of 150 μmol photons m^{-2} s^{-1} (630-nm peak) to accurately capture decreasing PSII photochemistry in HL. Saturating pulses of 200 ms provided the same actinic LEDs were used throughout (15 mmol photons m^{-2} s^{-1}), and the resulting F_M and F_M' values were used to calculate the q_I parameter according to the Stern-Volmer quenching approximation: NPQ = $(F_M - F_M')/F_M'$ in the absence of other quenchers. The cells were spun during the measurements with a magnetic stirrer. Steady-state fluorescence parameters were corrected to exclude the PSI contribution (3% at F_M) in data shown in Fig. 5 to account for the absence of PSI in the model membranes.

In absorption mode, P_{700} and plastocyanin redox changes were monitored upon dark pulse using detecting flashes passing through 705-nm (10-nm FWHM) and 730-nm (10-nm FWHM) filters, respectively, and the actinic light was cut from the detectors with Schott RG695 long-pass filters. DCMU (10 μM) was added for P_{700} experiments.

PSI:PSII ratio and PSII antenna size were determined using electrochromic shift measurements as described previously (*11*, *13*).

Oxygen emission recordings were done simultaneously with fluorescence measurements using a micro-optode (UniSense) stuck inside the culture cuvette. The optode was calibrated in Min medium flushed with air (O_2 saturated) and in the presence of glucose and glucose oxidase (anoxia).

Cell absorption spectra were measured using a Cary 4000 spectrophotometer (Varian) fitted with a diffuse reflectance accessory to account for light scattering.

Fluorescence spectra of cells and of BN gel pieces at 77 K were measured with an F-CCDZEN fluorimeter (JBeamBio). A LED peaking at 470 nm was used for the excitation.

Time-resolved fluorescence (Fig. 5 and fig. S3) was recorded at room temperature with a time-correlated single-photon counting setup (FluoTime 200, PicoQuant). A 10 mm by 10 mm quartz cuvette was used, and the cells were stirred using a magnetic stirrer during the measurements. Excitation was provided by a 438-nm laser working at a 10-MHz repetition rate and was set to 30 μW using a neutral density filter. A long-pass optical filter was placed in front of the detector to prevent scattered light from reaching the photodiode. Detection was done at 680 ± 8 nm with 4-ps bins. DCMU (10 μM) was added to close PSII (F_M state). The instrument response function (IRF) was measured through the decay of pinacyanol iodide in methanol (6-ps lifetime). IRF obtained was 88-ps FWHM under the same conditions as sample measurements. Data analysis was done with the FluoFit software, and the decays were deconvoluted with the IRF and three exponential decay functions to yield $\tau_{average}$ values. In Fig. 5 (N and P), the PSI-related component (~60 ps) was excluded from the plot to uniquely show the PSII-related contribution to fluorescence decay.

Streak camera measurements (Fig. 1 and figs. S15 to S18) at room temperature were done as described previously (*11*). Sample was stirred during the measurements. A 400-nm laser excitation was used (Vitesse Duo, Coherent), and the power at the ~50-μm-diameter spot was set to 15 μW with a 250-MHz repetition rate. DCMU (10 μM) was added to close PSII (F_M state). Averages of 100 images (10-s integration each) were background- and shading-corrected.

Global analysis of the streak camera images was done as described in (*83*). GloTarAn software was used for the data analysis (*84*), and linked analysis of three biological replicas each at three time points of photoinhibition was performed.

Biochemistry

Total protein extracts and thylakoids were isolated as described in (*85*). BN-PAGE was performed according to (*86*). The resolving gel of BN-PAGE used was 4.1 to 14% T (w/v), while the stacking gel was 3.6% T (w/v), where T stands for the total concentration of acrylamide and bisacrylamide monomers. Blue-native gels were cut into strips and loaded onto an SDS gel for the second dimension. Four percent T (w/v) was used for the stacking gel and 12% T (w/v) for the resolving gel. After running, the gels were either stained with a Coomassie blue solution (0.1% Coomassie blue R250 in 10% acetic acid, 40% methanol, and 50% H_2O) for 2 hours and destained with a destaining solution (10% acetic acid, 40% methanol, and 50% H_2O) for 3 × 2 hours or used for immunoblotting.

Immunoblotting was performed as described in (*87*). One microgram of Chl thylakoid or total protein extract was loaded onto a precast gel [4 to 12% T (w/v) Bis-Tris Plus, Invitrogen]. After electrophoresis, the proteins were transferred to a nitrocellulose membrane. The SDS gel after two-dimensional BN-PAGE was also used for the protein transfer procedure. The membrane was then blocked with 10% (w/v) milk in TTBS [20 mM tris (pH 7.5), 150 mM NaCl, and 0.1% Tween 20] for 1 hour and then incubated with different primary antibodies overnight in the dark at 4°C. All antibodies were purchased from Agrisera. The membrane was then washed with TTBS for 4 × 10 min and was incubated with the secondary antibody (goat anti-rabbit immunoglobulin G) for another 1 hour. The membrane was rewashed with TTBS for 4 × 5 min and was developed for chemiluminescence (with agent SuperSignal West Pico, Thermo Fisher Scientific) using a LAS 4000 Image Analyzer (ImageQuant).

Modeling

The excitation energy transfer rate matrix was constructed using a membrane model originally developed for *Arabidopsis thaliana* (*48*). Excitation energy transfer was simulated using generalized Forster theory combined with a collection of previously described Hamiltonians and protein structures (*48*). Open (k_{cs} = 1.56 ps^{-1}, k_{rc} = 0.00625 ps^{-1}, and k_{irr} = 0.00192 ps^{-1}) and closed (k_{cs} = 0.00323 ps^{-1} and k_{rc} = 0.00218 ps^{-1}) RCs had the same electron transport rates as

reported previously (*48*, *49*). Damaged RCs, which are incapable of charge separation, are either broken and have no additional rates of transport or quenching in which case a new loss channel arises with a rate of k_{qI}. All calculations presented in the Results section use $k_{qI} = 0.1\ ps^{-1}$. To construct a rate matrix for a specified number of open, closed, broken, and quenching RCs, a random number generator was used to determine which of the 128 RCs in the membrane belonged to each type. For F_M (F_0) simulations, the number of open (closed) RCs is taken to be 0. Last, the time evolution of the excitation population was simulated using

$$dP(t)/dt = KP(t)$$

and a fourth order Runge-Kutta integration method with time steps 0.2 ps. The excitation population was time evolved to 6 ns where residual chlorophyll excitation was negligible. The steady-state fluorescence observables were computed using the simulated fluorescence yield and then averaged over 20 realizations of RC assignments that satisfy the population distribution determined from the kinetic model.

SUPPLEMENTARY MATERIALS

Supplementary material for this article is available at https://science.org/doi/10.1126/sciadv.abj0055

View/request a protocol for this paper from *Bio-protocol*.

REFERENCES AND NOTES

1. W. Wietrzynski, M. Schaffer, D. Tegunov, S. Albert, A. Kanazawa, J. M. Plitzko, W. Baumeister, B. D. Engel, Charting the native architecture of *Chlamydomonas* thylakoid membranes with single-molecule precision. *eLife* **9**, e53740 (2020).
2. R. Croce, H. van Amerongen, Light harvesting in oxygenic photosynthesis: Structural biology meets spectroscopy. *Science* **369**, eaay2058 (2020).
3. L. Shen, Z. Huang, S. Chang, W. Wang, J. Wang, T. Kuang, G. Han, J.-R. Shen, X. Zhang, Structure of a $C_2S_2M_2N_2$-type PSII–LHCII supercomplex from the green alga *Chlamydomonas reinhardtii*. *Proc. Natl. Acad. Sci. U.S.A.* **116**, 21246–21255 (2019).
4. D. I. G. Bennett, G. R. Fleming, K. Amarnath, Energy-dependent quenching adjusts the excitation diffusion length to regulate photosynthetic light harvesting. *Proc. Natl. Acad. Sci. U.S.A.* **115**, E9523–E9531 (2018).
5. P. Joliot, A. Joliot, Etude cinétique de la réaction photochimique libérant l'oxygène au cours de la photosynthèse. *C. R. Hebd. Seances Acad. Sci.* **258**, 4622–4625 (1964).
6. K. Brinkert, S. De Causmaecker, A. Krieger-Liszkay, A. Fantuzzi, A. W. Rutherford, Bicarbonate-induced redox tuning in photosystem II for regulation and protection. *Proc. Natl. Acad. Sci. U.S.A.* **113**, 12144–12149 (2016).
7. G. N. Johnson, A. W. Rutherford, A. Krieger, A change in the midpoint potential of the quinone Q_A in Photosystem II associated with photoactivation of oxygen evolution. *Biochim. Biophys. Acta Bioenerg.* **1229**, 202–207 (1995).
8. A. W. Rutherford, A. Osyczka, F. Rappaport, Back-reactions, short-circuits, leaks and other energy wasteful reactions in biological electron transfer: Redox tuning to survive life in O_2. *FEBS Lett.* **586**, 603–616 (2012).
9. G. Peers, T. B. Truong, E. Ostendorf, A. Busch, D. Elrad, A. R. Grossman, M. Hippler, K. K. Niyogi, An ancient light-harvesting protein is critical for the regulation of algal photosynthesis. *Nature* **462**, 518–521 (2009).
10. T. Roach, C. S. Na, W. Stöggl, A. Krieger-Liszkay, The non-photochemical quenching protein LHCSR3 prevents oxygen-dependent photoinhibition in *Chlamydomonas reinhardtii*. *J. Exp. Bot.* **71**, 2650–2660 (2020).
11. L. Tian, W. J. Nawrocki, X. Liu, I. Polukhina, I. H. M. van Stokkum, R. Croce, pH dependence, kinetics and light-harvesting regulation of nonphotochemical quenching in *Chlamydomonas*. *Proc. Natl. Acad. Sci. U.S.A.* **116**, 8320–8325 (2019).
12. R. Croce, Beyond 'seeing is believing': The antenna size of the photosystems in vivo. *New Phytol.* **228**, 1214–1218 (2020).
13. W. J. Nawrocki, S. Santabarbara, L. Mosebach, F.-A. Wollman, F. Rappaport, State transitions redistribute rather than dissipate energy between the two photosystems in *Chlamydomonas*. *Nat. Plants* **2**, 16031 (2016).
14. B. Kok, On the inhibition of photosynthesis by intense light. *Biochim. Biophys. Acta* **21**, 234–244 (1956).
15. R. Kale, A. E. Hebert, L. K. Frankel, L. Sallans, T. M. Bricker, P. Pospíšil, Amino acid oxidation of the D1 and D2 proteins by oxygen radicals during photoinhibition of Photosystem II. *Proc. Natl. Acad. Sci. U.S.A.* **114**, 2988–2993 (2017).
16. I. Ohad, D. J. Kyle, C. J. Arntzen, Membrane protein damage and repair: Removal and replacement of inactivated 32-kilodalton polypeptides in chloroplast membranes. *J. Cell Biol.* **99**, 481–485 (1984).
17. E.-M. Aro, I. Virgin, B. Andersson, Photoinhibition of Photosystem II. Inactivation, protein damage and turnover. *Biochim. Biophys. Acta Bioenerg.* **1143**, 113–134 (1993).
18. N. Murata, S. Takahashi, Y. Nishiyama, S. I. Allakhverdiev, Photoinhibition of photosystem II under environmental stress. *Biochim. Biophys. Acta Bioenerg.* **1767**, 414–421 (2007).
19. E. Tyystjärvi, Photoinhibition of Photosystem II, in *International Review of Cell and Molecular Biology* (Elsevier, 2013), vol. 300, pp. 243–303;https://linkinghub.elsevier.com/retrieve/pii/B9780124052109000072.
20. I. Vass, K. Cser, Janus-faced charge recombinations in photosystem II photoinhibition. *Trends Plant Sci.* **14**, 200–205 (2009).
21. S. P. Long, S. Humphries, P. G. Falkowski, Photoinhibition of photosynthesis in nature. *Annu. Rev. Plant. Physiol. Plant. Mol. Biol.* **45**, 633–662 (1994).
22. E. A. Ainsworth, D. R. Ort, How do we improve crop production in a warming world? *Plant Physiol.* **154**, 526–530 (2010).
23. A. Zavafer, A theoretical framework of the hybrid mechanism of photosystem II photodamage. *Photosynth. Res.* **149**, 107–120 (2021).
24. M. Hakala, I. Tuominen, M. Keränen, T. Tyystjärvi, E. Tyystjärvi, Evidence for the role of the oxygen-evolving manganese complex in photoinhibition of Photosystem II. *Biochim. Biophys. Acta Bioenerg.* **1706**, 68–80 (2005).
25. N. Ohnishi, S. I. Allakhverdiev, S. Takahashi, S. Higashi, M. Watanabe, Y. Nishiyama, N. Murata, Two-step mechanism of photodamage to photosystem II: Step 1 occurs at the oxygen-evolving complex and step 2 occurs at the photochemical reaction center. *Biochemistry* **44**, 8494–8499 (2005).
26. A. U. Rehman, K. Cser, L. Sass, I. Vass, Characterization of singlet oxygen production and its involvement in photodamage of Photosystem II in the cyanobacterium Synechocystis PCC 6803 by histidine-mediated chemical trapping. *Biochim. Biophys. Acta Bioenerg.* **1827**, 689–698 (2013).
27. A. Krieger, I. Moya, E. Weis, Energy-dependent quenching of chlorophyll a fluorescence: Effect of pH on stationary fluorescence and picosecond-relaxation kinetics in thylakoid membranes and Photosystem II preparations. *Biochim. Biophys. Acta Bioenerg.* **1102**, 167–176 (1992).
28. S. Matsubara, W. S. Chow, Populations of photoinactivated photosystem II reaction centers characterized by chlorophyll a fluorescence lifetime in vivo. *Proc. Natl. Acad. Sci.* **101**, 18234–18239 (2004).
29. M. Richter, R. Goss, B. Wagner, A. R. Holzwarth, Characterization of the fast and slow reversible components of non-photochemical quenching in isolated pea thylakoids by picosecond time-resolved chlorophyll fluorescence analysis. *Biochemistry* **38**, 12718–12726 (1999).
30. A. Zavafer, I. Iermak, M. H. Cheah, W. S. Chow, Two quenchers formed during photodamage of phostosystem II and the role of one quencher in preemptive photoprotection. *Sci. Rep.* **9**, 17275 (2019).
31. N. R. Baker, Chlorophyll fluorescence: A probe of photosynthesis in vivo. *Annu. Rev. Plant Biol.* **59**, 89–113 (2008).
32. H. Kautsky, A. Hirsch, Neue Versuche zur Kohlensäureassimilation. *Naturwissenschaften* **19**, –964 (1931).
33. D. Lazár, Chlorophyll *a* fluorescence induction. *Biochim. Biophys. Acta Bioenerg.* **1412**, 1–28 (1999).
34. F. A. Wollman, J. Olive, P. Bennoun, M. Recouvreur, Organization of the photosystem II centers and their associated antennae in the thylakoid membranes: A comparative ultrastructural, biochemical, and biophysical study of Chlamydomonas wild type and mutants lacking in photosystem II reaction centers. *J. Cell Biol.* **87**, 728–735 (1980).
35. E. Dinc, L. Tian, L. M. Roy, R. Roth, U. Goodenough, R. Croce, LHCSR1 induces a fast and reversible pH-dependent fluorescence quenching in LHCII in *Chlamydomonas reinhardtii* cells. *Proc. Natl. Acad. Sci. U.S.A.* **113**, 7673–7678 (2016).
36. N. Depège, S. Bellafiore, J.-D. Rochaix, Role of chloroplast protein kinase Stt7 in LHCII phosphorylation and state transition in *Chlamydomonas*. *Science* **299**, 1572–1575 (2003).
37. P. Bag, V. Chukhutsina, Z. Zhang, S. Paul, A. G. Ivanov, T. Shutova, R. Croce, A. R. Holzwarth, S. Jansson, Direct energy transfer from photosystem II to photosystem I confers winter sustainability in Scots Pine. *Nat. Commun.* **11**, 6388 (2020).
38. P. Horton, M. Wentworth, A. Ruban, Control of the light harvesting function of chloroplast membranes: The LHCII-aggregation model for non-photochemical quenching. *FEBS Lett.* **579**, 4201–4206 (2005).
39. Y. Miloslavina, A. Wehner, P. H. Lambrev, E. Wientjes, M. Reus, G. Garab, R. Croce, A. R. Holzwarth, Far-red fluorescence: A direct spectroscopic marker for LHCII oligomer formation in non-photochemical quenching. *FEBS Lett.* **582**, 3625–3631 (2008).

40. S. D. Gallaher, S. T. Fitz-Gibbon, A. G. Glaesener, M. Pellegrini, S. S. Merchant, Chlamydomonas genome resource for laboratory strains reveals a mosaic of sequence variation, identifies true strain histories, and enables strain-specific studies. *Plant Cell* **27**, 2335–2352 (2015).
41. Y. Kato, X. Sun, L. Zhang, W. Sakamoto, Cooperative D1 degradation in the photosystem II repair mediated by chloroplastic proteases in Arabidopsis. *Plant Physiol.* **159**, 1428–1439 (2012).
42. A. Malnoë, F. Wang, J. Girard-Bascou, F.-A. Wollman, C. de Vitry, Thylakoid FtsH protease contributes to photosystem II and cytochrome b_6f remodeling in *Chlamydomonas reinhardtii* under stress conditions. *Plant Cell* **26**, 373–390 (2014).
43. F. Wang, Y. Qi, A. Malnoë, Y. Choquet, F.-A. Wollman, C. de Vitry, The high light response and redox control of thylakoid FtsH protease in *Chlamydomonas reinhardtii*. *Mol. Plant* **10**, 99–114 (2017).
44. L. Tian, E. Dinc, R. Croce, LHCII populations in different quenching states are present in the thylakoid membranes in a ratio that depends on the light conditions. *J. Phys. Chem. Lett.* **6**, 2339–2344 (2015).
45. M. Lingvay, P. Akhtar, K. Sebők-Nagy, T. Páli, P. H. Lambrev, Photobleaching of chlorophyll in light-harvesting complex II increases in lipid environment. *Front. Plant Sci.* **11**, e00849 (2020).
46. H. S. Gong, I. Ohad, The PQ/PQH2 ratio and occupancy of photosystem II-QB site by plastoquinone control the degradation of D1 protein during photoinhibition in vivo. *J. Biol. Chem.* **266**, 21293–21299 (1991).
47. B. B. Fischer, R. I. L. Eggen, A. Trebst, A. Krieger-Liszkay, The glutathione peroxidase homologous gene Gpxh in Chlamydomonas reinhardtii is upregulated by singlet oxygen produced in photosystem II. *Planta* **223**, 583–590 (2006).
48. K. Amarnath, D. I. G. Bennett, A. R. Schneider, G. R. Fleming, Multiscale model of light harvesting by photosystem II in plants. *Proc. Natl. Acad. Sci. U.S.A.* **113**, 1156–1161 (2016).
49. D. I. G. Bennett, K. Amarnath, G. R. Fleming, A structure-based model of energy transfer reveals the principles of light harvesting in photosystem II supercomplexes. *J. Am. Chem. Soc.* **135**, 9164–9173 (2013).
50. G. D. Scholes, Long-range resonance energy transfer in molecular systems. *Annu. Rev. Phys. Chem.* **54**, 57–87 (2003).
51. J.-H. Chen, S.-T. Chen, N.-Y. He, Q.-L. Wang, Y. Zhao, W. Gao, F.-Q. Guo, Nuclear-encoded synthesis of the D1 subunit of photosystem II increases photosynthetic efficiency and crop yield. *Nat. Plants* **6**, 570–580 (2020).
52. W. S. Chow, E.-M. Aro, Photoinactivation and mechanisms of recovery, in *Photosystem II: The Light-Driven Water:Plastoquinone Oxidoreductase*, T. J. Wydrzynski, K. Satoh, J. A. Freeman, Eds. (Advances in Photosynthesis and Respiration, Springer Netherlands, 2005), pp. 627–648;https://doi.org/10.1007/1-4020-4254-X_28.
53. M. Hippler, K. Redding, J.-D. Rochaix, *Chlamydomonas* genetics, a tool for the study of bioenergetic pathways. *Biochim. Biophys. Acta Bioenerg.* **1367**, 1–62 (1998).
54. R. Oguchi, I. Terashima, W. S. Chow, The involvement of dual mechanisms of photoinactivation of photosystem II in *Capsicum annuum* L. plants. *Plant Cell Physiol.* **50**, 1815–1825 (2009).
55. É. Hideg, C. Spetea, I. Vass, Singlet oxygen and free radical production during acceptor- and donor-side-induced photoinhibition: Studies with spin trapping EPR spectroscopy. *Biochim. Biophys. Acta Bioenerg.* **1186**, 143–152 (1994).
56. R. Oguchi, I. Terashima, J. Kou, W. S. Chow, Operation of dual mechanisms that both lead to photoinactivation of photosystem II in leaves by visible light. *Physiol. Plant.* **142**, 47–55 (2011).
57. Y. Takegawa, M. Nakamura, S. Nakamura, T. Noguchi, J. Sellés, A. W. Rutherford, A. Boussac, M. Sugiura, New insights on Chl_{D1} function in photosystem II from site-directed mutants of D1/T179 in *Thermosynechococcus elongatus*. *Biochim. Biophys. Acta Bioenerg.* **1860**, 297–309 (2019).
58. S. Santabarbara, I. Cazzalini, A. Rivadossi, F. M. Garlaschi, G. Zucchelli, R. C. Jennings, Photoinhibition in vivo and in vitro Involves weakly coupled chlorophyll–protein complexes. *Photochem. Photobiol.* **75**, 613–618 (2002).
59. M. Hakala-Yatkin, M. Mäntysaari, H. Mattila, E. Tyystjärvi, Contributions of visible and ultraviolet parts of sunlight to photoinhibition. *Plant Cell Physiol.* **51**, 1745–1753 (2010).
60. Y. Nishiyama, S. I. Allakhverdiev, N. Murata, A new paradigm for the action of reactive oxygen species in the photoinhibition of photosystem II. *Biochim. Biophys. Acta Bioenerg.* **1757**, 742–749 (2006).
61. T. Roach, A. Krieger-Liszkay, Photosynthetic regulatory mechanisms for efficiency and prevention of photo-oxidative stress, in *Annual Plant Reviews online* (American Cancer Society, 2019), pp. 273–306;https://onlinelibrary.wiley.com/doi/abs/10.1002/9781119312994.apr0666.
62. S. Santabarbara, I. Cazzalini, R. Barbato, D. Tarantino, G. Zucchelli, F. Garlaschi, R. Jennings, Is non photochemical quenching protective? *Science Access* **3**, sa0403086 (2001).
63. P. Sarvikas, T. Tyystjärvi, E. Tyystjärvi, Kinetics of prolonged photoinhibition revisited: Photoinhibited photosystem II centres do not protect the active ones against loss of oxygen evolution. *Photosynth. Res.* **103**, 7–17 (2010).
64. J. Zabret, S. Bohn, S. K. Schuller, O. Arnolds, M. Möller, J. Meier-Credo, P. Liauw, A. Chan, E. Tajkhorshid, J. D. Langer, R. Stoll, A. Krieger-Liszkay, B. D. Engel, T. Rudack, J. M. Schuller, M. M. Nowaczyk, Structural insights into photosystem II assembly. *Nat. Plants* **7**, 524–538 (2021).
65. J. Kromdijk, K. Głowacka, L. Leonelli, S. T. Gabilly, M. Iwai, K. K. Niyogi, S. P. Long, Improving photosynthesis and crop productivity by accelerating recovery from photoprotection. *Science* **354**, 857–861 (2016).
66. E. Baena-González, R. Barbato, E.-M. Aro, Role of phosphorylation in the repair cycle and oligomeric structure of photosystem II. *Planta* **208**, 196–204 (1999).
67. L. Li, E.-M. Aro, A. H. Millar, Mechanisms of photodamage and protein turnover in photoinhibition. *Trends Plant Sci.* **23**, 667–676 (2018).
68. C. A. Shipton, J. Barber, In vivo and in vitro photoinhibition reactions generate similar degradation fragments of D1 and D2 photosystem-II reaction-centre proteins. *Eur. J. Biochem.* **220**, 801–808 (1994).
69. B. Ke, The primary electron donor of photosystem II, P680, and photoinhibition, in *Photosynthesis: Photobiochemistry and Photobiophysics* (Advances in Photosynthesis and Respiration, Springer Netherlands, 2001), pp. 271–288;https://doi.org/10.1007/0-306-48136-7_15.
70. M. J. Davies, Singlet oxygen-mediated damage to proteins and its consequences. *Biochem. Biophys. Res. Commun.* **305**, 761–770 (2003).
71. B. Andersson, E.-M. Aro, Photodamage and D1 protein turnover in Photosystem II, in *Regulation of Photosynthesis*, E.-M. Aro, B. Andersson, Eds. (Advances in Photosynthesis and Respiration, Springer Netherlands, 2001), pp. 377–393;https://doi.org/10.1007/0-306-48148-0_22.
72. E. Kapri-Pardes, L. Naveh, Z. Adam, The thylakoid lumen protease Deg1 is involved in the repair of photosystem II from photoinhibition in *Arabidopsis*. *Plant Cell* **19**, 1039–1047 (2007).
73. J. Theis, J. Lang, B. Spaniol, S. Ferté, J. Niemeyer, F. Sommer, D. Zimmer, B. Venn, S. F. Mehr, T. Mühlhaus, F.-A. Wollman, M. Schroda, The *Chlamydomonas deg1c* mutant accumulates proteins involved in high light acclimation. *Plant Physiol.* **181**, 1480–1497 (2019).
74. Y. Eisenberg-Domovich, R. Oelmüller, R. G. Herrmann, I. Ohad, Role of the RCII-D1 protein in the reversible association of the oxygen-evolving complex proteins with the lumenal side of photosystem II. *J. Biol. Chem.* **270**, 30181–30186 (1995).
75. T. Hundal, I. Virgin, S. Styring, B. Andersson, Changes in the organization of photosystem II following light-induced D_1-protein degradation. *Biochim. Biophys. Acta Bioenerg.* **1017**, 235–241 (1990).
76. M. Uthoff, U. Baumann, Conformational flexibility of pore loop-1 gives insights into substrate translocation by the AAA+ protease FtsH. *J. Struct. Biol.* **204**, 199–206 (2018).
77. C. de Vitry, J. Olive, D. Drapier, M. Recouvreur, F. A. Wollman, Posttranslational events leading to the assembly of photosystem II protein complex: A study using photosynthesis mutants from *Chlamydomonas reinhardtii*. *J. Cell Biol.* **109**, 991–1006 (1989).
78. L. Minai, K. Wostrikoff, F.-A. Wollman, Y. Choquet, Chloroplast biogenesis of photosystem II cores involves a series of assembly-controlled steps that regulate translation. *Plant Cell* **18**, 159–175 (2006).
79. H. Kirst, J. G. Garcia-Cerdan, A. Zurbriggen, T. Ruehle, A. Melis, Truncated photosystem chlorophyll antenna size in the green microalga *Chlamydomonas reinhardtii* upon deletion of the *TLA3-CpSRP43* gene. *Plant Physiol.* **160**, 2251–2260 (2012).
80. S. Bujaldon, N. Kodama, M. K. Rathod, N. Tourasse, S.-I. Ozawa, J. Sellés, O. Vallon, Y. Takahashi, F.-A. Wollman, The BF4 and *p71* antenna mutants from *Chlamydomonas reinhardtii*. *Biochim. Biophys. Acta Bioenerg.* **1861**, 148085 (2020).
81. P. Bennoun, M. Spierer-Herz, J. Erickson, J. Girard-Bascou, Y. Pierre, M. Delosme, J.-D. Rochaix, Characterization of photosystem II mutants of *Chlamydomonas reinhardii* lacking the psbA gene. *Plant Mol. Biol.* **6**, 151–160 (1986).
82. D. Dauvillée, O. Stampacchia, J. Girard-Bascou, J.-D. Rochaix, Tab2 is a novel conserved RNA binding protein required for translation of the chloroplast psaB mRNA. *EMBO J.* **22**, 6378–6388 (2003).
83. I. H. M. van Stokkum, Systems biophysics: Global and target analysis of light harvesting and photochemical quenching in vivo, in *Light Harvesting in Photosynthesis*, R. Croce, R. van Grondelle, H. van Amerongen, I. van Stokkum, Eds. (CRC Press, 2018), pp. 467–482.
84. J. J. Snellenburg, S. Laptenok, R. Seger, K. M. Mullen, I. H. M. van Stokkum, Glotaran: A Java-based graphical user interface for the R package TIMP. *J. Stat. Softw.* **49**, 1–22 (2012).
85. S. Ramundo, M. Rahire, O. Schaad, J.-D. Rochaix, Repression of essential chloroplast genes reveals new signaling pathways and regulatory feedback loops in *Chlamydomonas*. *Plant Cell* **25**, 167–186 (2013).
86. Y. Chen, Y. Shimoda, M. Yokono, H. Ito, A. Tanaka, Mg-dechelatase is involved in the formation of photosystem II but not in chlorophyll degradation in *Chlamydomonas reinhardtii*. *Plant J.* **97**, 1022–1031 (2019).
87. W. J. Nawrocki, X. Liu, R. Croce, *Chlamydomonas reinhardtii* exhibits de facto constitutive NPQ capacity in physiologically relevant conditions. *Plant Physiol.* **182**, 472–479 (2020).

88. P. Virtanen, R. Gommers, T. E. Oliphant, M. Haberland, T. Reddy, D. Cournapeau, E. Burovski, P. Peterson, W. Weckesser, J. Bright, S. J. van der Walt, M. Brett, J. Wilson, K. J. Millman, N. Mayorov, A. R. J. Nelson, E. Jones, R. Kern, E. Larson, C. J. Carey, İ. Polat, Y. Feng, E. W. Moore, J. V. Plas, D. Laxalde, J. Perktold, R. Cimrman, I. Henriksen, E. A. Quintero, C. R. Harris, A. M. Archibald, A. H. Ribeiro, F. Pedregosa, P. van Mulbregt; SciPy 1.0 Contributors, SciPy 1.0: Fundamental algorithms for scientific computing in Python. *Nat. Methods* **17**, 261–272 (2020).

Acknowledgments: S. Bujaldon is acknowledged for help with the crossing. We thank A. Malnoë for helpful comments. **Funding:** This work was supported by European Commission Marie Skłodowska-Curie fellowship xFATE 799083 (W.J.N.), Netherlands Organization for Scientific Research TOP grant 714.018.001 (R.C.), Chinese Scholarship Council fellowship 201606910042 (X.L.), Southern Methodist University startup funds (B.R. and D.I.G.B.), French National Centre for Scientific Research basic support (C.d.V.), and French National Research Agency grant DYNAMO ANR-11-LABX-0011-01 (C.d.V.). **Author contributions:** Methodology: W.J.N., B.R., and D.I.G.B. Software: B.R. and D.I.G.B. Investigation: W.J.N., X.L., C.H., and C.d.V. Writing—original draft: W.J.N. Writing—review and editing: all authors. Conceptualization: W.J.N. and R.C. Supervision and funding acquisition: W.J.N., D.I.G.B., and R.C. **Competing interests:** The authors declare that they have no competing interests. **Data and materials availability:** All data needed to evaluate the conclusions in the paper are present in the paper and/or the Supplementary Materials.

Submitted 14 April 2021
Accepted 8 November 2021
Published 22 December 2021
10.1126/sciadv.abj0055

ScienceAdvances

Molecular origins of induction and loss of photoinhibition-related energy dissipation q

Wojciech J. NawrockiXin LiuBailey RaberChen HuCatherine de VitryDoran I. G. BennettRoberta Croce

Sci. Adv., 7 (52), eabj0055. • DOI: 10.1126/sciadv.abj0055